NUMERICAL SIMULATIONS OF KCS SELF-PROPULSION AND ZIGZAG MANEUVER BY URANS-OVERSET GRID METHOD

Zhen Ren, Jianhua Wang, Decheng Wan*
Computational Marine Hydrodynamics Lab (CMHL), State Key Laboratory of Ocean Engineering, School of Naval Architecture, Ocean and Civil Engineering, Shanghai Jiao Tong University, Shanghai, China
***Corresponding author: dcwan@sjtu.edu.cn**

1. INTRODUCTION

It is very complex to carry out the numerical simulations of self-propulsion and zigzag maneuver of ship with full appendages. The flow field of KCS self-propulsion and zigzag maneuver at Fr=0.26 is solved by URANS equations and overset grid method. In the simulations of self-propulsion, the sinkage and pitch of the hull are taken into account. The rotation speed of propeller is obtained by PI controller. And the predicted speed of propeller is about 12.44rps. The fixed rotating speed is adopted in the 10/10 and 20/20 zigzag maneuver. The predicted results are in good agreement with the experiments. The wake field, dynamic pressure and vorticity are presented at to analyze the flow mechanism.

In the current studies on the ship hydrodynamic performance, one of the most complex issues is the matching of hull, propeller and rudder. The propeller and rudder will move with the hull, while they also rotates in the local coordinate system. The wake field and pressure distribution on hull is affected by the suction effect of propeller. And the variation in the wake field will affect both the thrust of propeller and the lateral force of rudder. The attitude and navigation direction of ship is going to be affected due to executing the rudder. The variation of the sailing attitude of ship will be accompanied by the drastic change of the wake field, which further affects the propulsion efficiency of the propeller and the steering moment of the rudder. The lift of rudder is also influenced by the drastic variation of wake field produced by propeller. It is obvious that their roles are mutually coupled.

In the research of the matching of hull, propeller, and rudder, computational fluid dynamics (CFD) is one of the most effective method to obtain more accurate results and detailed flow field information. In early study, the body force propeller method was widely used due to the simplicity and small amount of calculation. In 1988, Stern [1] realized the numerical simulations of hull-propeller interaction by using body force propeller. Phillips et al. [2] calculated the hull-propeller interaction of KVLCC2 at a fixed rudder angle by coupling RANS and Blade element momentum theory, and used this method to calculate the hydrodynamic derivative. Choi et al. [3][4] combined the vortex lattice method with the commercial CFD software, FLUENT, to carry out the numerical predictions on the matching of multiple hulls with propellers. Although this method is used widely, the accuracy of numerical simulations is limited since the real geometry of propellers are not taken into consideration.

In terms of predicted accuracy of the body force method, researchers have begun to generate the grid of the real propeller directly. And sliding mesh method is used gradually. In 2005, Lübke[5] used commercial software, CFX and sliding mesh method to perform self-propulsion simulations of KCS on a fixed attitude. Shen and Su [6] predicted the hull-propeller interaction of KCS based on DES method and sliding mesh method. Wang et al. [7] preformed the numerical simulations of rotating arm tests of MARIN 7963 by coupling MRF method for steady turning circle test of hull with sliding mesh method for the rotation of the twin propellers and analyzed the flow field around the hull, propeller and rudder.

Overset grid method can easily deal with complex motions, such as self-propulsion or maneuvers with

full appendages and it can also ensure the accuracy of the predicted results. Carrica and Stern [8] realized the numerical simulations of free running ship maneuvering motion by combining with the solver CFD Ship-Iwoa with overset mesh method. In their study, the zigzag maneuvering and turning circle test are of KVLCC are carried out. Mofidi and Carrica [9] used the same solver and numerical method to carry out the simulations of typical zigzag 10/10 and modified zigzag 15/1 maneuvering test. The predicted results are in good agreement with the experiment and the detailed flow field in the self-propulsion maneuvering motion is analyzed. Broglia et al. [10] and Dubbioso et al. [11] performed numerical simulations of the free turning circle test of a self-propelled ship with single rudder and twin rudders, respectively. They analyzed the rudder force and the variation of the lateral force acting on the hull and appendages. It is pointed that the load on the propellers was interfered strongly by the rudder, especially for twin propellers. Muscari et al. [12] simulated the pure yaw motion and free turning circle maneuvering of the hull with twin propellers and twin rudders by overset mesh. Based on the open source code platform OpenFOAM, Shen et al. [13][16] introduced the overset mesh to develop the solver suitable for naval architecture and ocean engineering, naoe-FOAM-SJTU. To verify the solver, they performed the numerical simulations of the self-propulsion and zigzag maneuvering of KCS, and the results show that the accurate predicted results were obtained in the numerical simulations. With this solver being used, Wang et al. [17]**错误!未找到引用源。** carried out extensive numerical simulations of the free-running ship maneuvering motion for the ONR Tumblehome ship model with twin propellers and twin rudders. The predicted characteristic parameters of maneuverability are in good agreement with the experimental results.

In the present study, the numerical simulation of self-propulsion and standard zigzag maneuver of KCS are carried out according to benchmark test in SIMMAN 2020. The paper is organized as follows. Numerical methods including the numerical schemes are illustrated. Then the geometry model of the hull, propeller and rudder, grid generation and test conditions are presented. The results of self-propulsion simulation are analyzed firstly and then the simulations of zigzag maneuvering are discussed subsequently. Finally, a brief conclusion is drawn.

2. NUMERICAL METHOD

The present simulations are carried out by the in-house CFD solver, naoe-FOAM-SJTU, which is developed based on the open source platform OpenFOAM. It is able to conduct the numerical simulations of the free-running ship maneuvering motion by coupling the dynamic overset grid and the 6DoF motion module that includes a hierarchy of bodies. In the present simulations, the Unsteady Reynolds-averaged Navier-Stokes equations are solved by the solver, naoe-FOAM-SJTU. The governing equations are as followed:

$$\nabla \cdot \mathbf{U} = 0 \tag{1}$$

$$\frac{\partial \rho \mathbf{U}}{\partial t} + \nabla \cdot \left(\rho(\mathbf{U} - \mathbf{U_g})\mathbf{U}\right) = -\nabla p_d - \mathbf{g} \cdot \mathbf{x} \nabla \rho + \nabla \cdot (\mu_{eff} \nabla \mathbf{U}) + (\nabla \mathbf{U}) \cdot \nabla \mu_{eff} + f_\sigma \tag{2}$$

where $\mathbf{U}$ and $\mathbf{U}_g$ represent fluid velocity field and the grid velocity, respectively; p_d is the dynamic pressure; ρ is the mixture density; $\boldsymbol{g}$ is the gravity acceleration; μ_{eff} is effective dynamic viscosity. f_σ is surface tension term.

The shear stress transport turbulence model is used to model the turbulence features accurately since the model combines the advantages of the standard k-ε model and k-ω model. In the prediction, the wall functions are used to simulate the velocity gradient effects near the wall. The volume of fluid (VOF) approach is adopted to capture the free surface. Phase fraction, α, indicates the relative proportion of different fluids in each cell and its definition is expressed as [20]:

$$\begin{cases} \alpha = 0 & air \\ \alpha = 1 & water \\ 0 < \alpha < 1 & interface \end{cases} \tag{3}$$

In the present simulations, the computational domain is divided into four parts, including background, hull, propeller and rudder domains for multi unstructured overset grids. The transformation between the physical and computational space is achieved by the finite volume method (FVM). And the

pressure-implicit split-operator (PISO) algorithm is applied to decouple the pressure-velocity in the governing equations.

Since the free-running ship maneuver is the large amplitude motion including the full appendages such as rotating propeller and turning rudder, it is necessary to use the dynamic overset technology and full 6DoF motion method with a hierarchy of bodies. The transformation between the overlapping grids is achieved by Suggar++ library. The variable in fringe cell is obtained by interpolating from the donor cells.

Since the appendages such as rotating propeller and turning rudder must be taken into consideration, the dynamic overset method should be coupled with the 6DoF motion module with a hierarchy of bodies. In the calculation, the hull advances according to the 6DoF equation and the propeller and rudder follow the hull with the same forward speed but can move in their own system. In the free-running ship motion, the background domain is the root level in the inertial system, and the hull domain is the parent level. The propeller or rudder are the children level and moves according their control laws firstly. And then they move together with the hull whose motion is obtained by 6DoF equation. At last, the background grid follows the hull motion, such as heave, roll and pitch, while the free surface keeps horizontal.

3. SIMULATION SETUP

3.1 Geometry model

According to the benchmark of CASE 3.2 in SIMMAN 2020, KRISO Container Ship is used in the present simulations. The hull is the 6.0702m replica with the KP505 propeller and rudder with NACA0018 section. Their geometry are shown in Figure 1, and the principle parameters are listed in Table 1. MARIN has conducted extensive experiments of free-running ship maneuvering motion for the ship model. In the present study, sinkage and pitch are taken into consideration in self-propulsion and the hull is free to move in all directions for zigzag maneuvering.

Figure 1 Geometry model of KCS

Table 1 Principle particulars of KCS

Main particulars	Symbols	Model scale 1:37.89
Length between perpendiculars	L_{pp}/m	6.0702
Beam	B_{WL}/m	0.8498
Draft	T/m	0.2850
Displacement volume	∇ /m^3	0.9571
Moment of Inertia	K_{xx}/B_{WL}	0.40
	K_{yy}/L_{pp} K_{zz}/L_{pp}	0.252
Diameter of propeller	D_p/m	0.2085
Propeller center, long. location (from FP)	x/L_{pp}	0.9825
Propeller center, vert. location (below WL)	$-z/L_{pp}$	0.02913
Propeller rotation direction (view from stern)		Clockwise
Rudder rate	deg/s	14.28

3.2 Grid Generation

In the present simulations, the unstructured grid is generated by HEXPRESS, which is the professional software for mesh generation developed by NUMECA. The computational domain and boundary condition are presented in Figure 2. The grids of background, hull, propeller and rudder are generated, respectively. The grid number and the hierarchy of each domain are listed in Table 2. The total grid number of the computational domain is about 6.07 million. And the propeller and rudder are the children level, which moves in the local coordinate system as they move with the hull. Figure 3 presents the local profile of hull, propeller and rudder grid and the surface mesh of propeller and rudder.

Table 2 Grid distribution in each part

Positon	Mesh number (million)	Hierarchy
Background	1.36	Root
Hull	3.56	Parent
Propeller	0.61	Children
Rudder	0.54	Children
Total	6.07	--

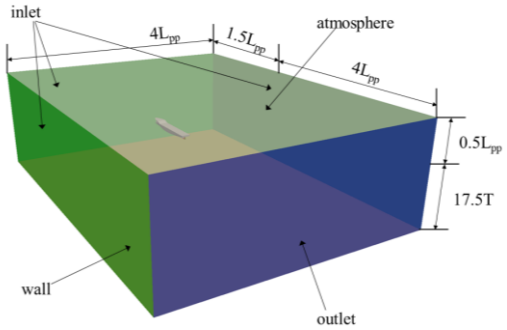

Figure 2 Computational domain and boundary condition

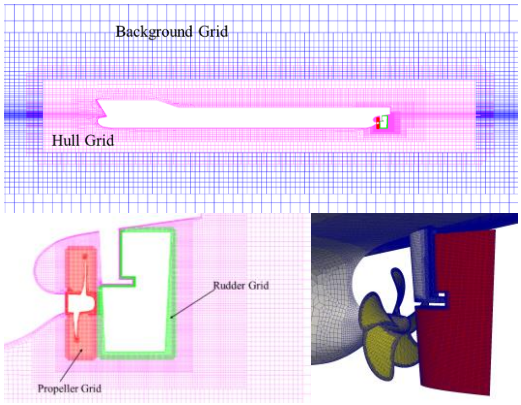

Figure 3 Grid distribution

3.3 Test conditions

All the simulations are setup according to the CASE3.2 in SIMMAN 2020. In the cases, CSAE 3.2.1 is for the self-propulsion and CASE 3.2.2 and CASE 3.2.3 are 10/10 and 20/20 zigzag maneuver. The starting speed of hull is 2.006m/s, corresponding to Fr=0.26. The gravitational acceleration, g, is 9.81m/s^2. The density of water is 1000kg/m^3. Kinematical viscosity coefficient, ν, is 1.27×10^{-6}m^2/s. All the simulations conditions are defined based on two non-dimensional number: the Reynold number $Re = V_0L_{WL}/\upsilon$ and the Froude number $Fr = V_0/gL_{WL}$, where υ is the kinematic viscosity, g is the

gravitational acceleration. All the computations of the free-running ship maneuver are at the same approaching speed of 2.006 m/s in model scale, corresponding to *Fr*=0.26.

4. RESULTS AND ANALYSIS

4.1 Self-propulsion

According to the experiments, the self-propulsion of the ship is performed with 6 degree of freedom. In the numerical simulations, the self-propulsion test is carried out to obtain the self-propulsion point. In the present study for self-propulsion, the rotation speed of propeller is obtained by PI controller, while fixed rotational speed is applied in the zigzag maneuver.

Figure 4 shows the time history of the rps of propeller and the hull speed obtained by PI controller. The predicted result of the propeller rotational speed is about 12.44 resolutions per second when the ship sails at a constant speed of 2.006m/s, corresponding to *Fr*=0.26. In the next simulations of zigzag maneuver, the rotational speed of propeller is kept constant for both cases.

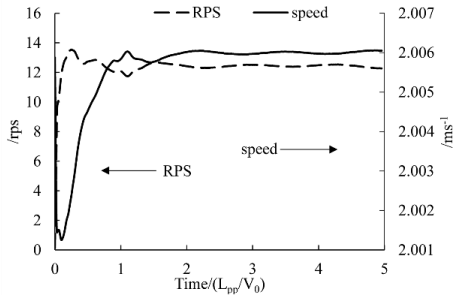

Figure 4 Time history of RPS and ship speed

The time history of the propeller thrust is depicted in Figure 5. As we can see, the mean value of the thrust is about 58.72N, and the torque is about 1.958NM. In one rotational cycle, five peaks are captured since the propeller owns five blades. The motion of the hull are shown in Figure 6, the ship sank about 0.121m and 0.154° trim by stern.

The wake field of hull-propeller-rudder is very complex, as shown in Figure 13. The top is the wake field in front of the propeller disk. It shows the inflow velocity of the propeller. The wake field is no more uniform due to the influence of the hull. The axial velocity is not axisymmetric and negative velocity appears in the center of the hull. The lateral velocity is roughly symmetrical along the center line of the hull. The positive velocity is mainly concentrated the portside and the negative mainly appears the starboard. And the high and low velocity mainly exits above the propeller shaft. The negative vertical velocity mainly appears above the propeller shaft, and the positive occurs below the shaft. The influence of the rudder on the wake field is more obviously, as shown in the bottom of Figure 13. The maximum and minimum of axial velocity appears on the starboard. The lateral velocity is roughly divided horizontally into two parts. The positive lateral velocity occurs above the shaft and the negative is concentrated below the shaft. While the vertical velocity is divided by the vertical plane, the positive velocity occurs on portside and the negative is on the starboard.

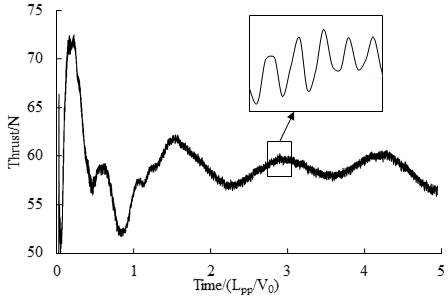

Figure 5 Time history of thrust of propeller

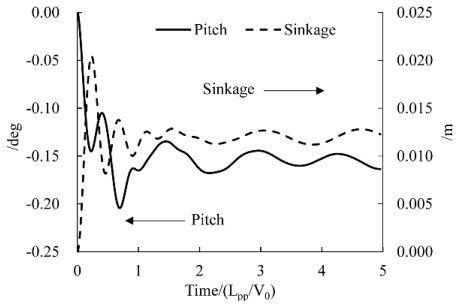

Figure 6 Time variation of pitch and sinkage

4.2 Zigzag maneuver

In the numerical simulations for zigzag maneuver, the rotational speed of propeller is kept constant and the rudder is controlled by PI controller. Both cases for 10/10 and 20/20 zigzag maneuver are simulated in the present studies. Figure 7 shows the comparison between the experimental and predicted rudder angle and yaw motion for 10/10 zigzag maneuver. And Table 3 lists the first and second overshoot angle and the time of maximum yaw angle. As we can see, good agreement between the experimental and predicted results are achieved in terms of overshoot angle and and the time to execute rudder. And the errors of first and second overshoot angles are 16.6% and -4.0%, respectively. Compared with the experimental results, the times to check yaw angle lag 9.35% and 5.31%, respectively. This is mainly because that the rotational speed of propellers is adopted in the present simulations that affects the speed of the hull directly and leads to the error of overshoot angel and the time to check yaw angle. A, B and C represent the time to start to execute rudder, end to execute rudder thirdly and the second overshoot angle. The flow field at this three times will be analyzed in the next.

Table 3 Comparison of main parameters for 10/10 zigzag maneuver

Parameters	EFD	CFD
1st OSA (deg)	10.76	12.55
2nd OSA (deg)	20.23	19.42
T (1st OSA) (L_{pp}/V_0)	3.53	3.86
T (2nd OSA) (L_{pp}/V_0)	9.41	9.91

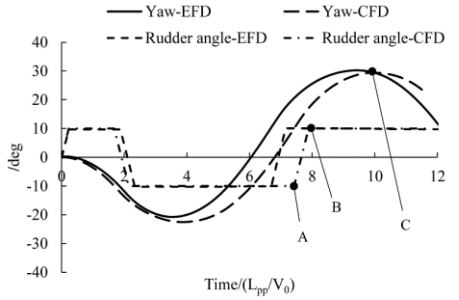

Figure 7 Time history of rudder angle and yaw motion for 10/10 zigzag maneuver

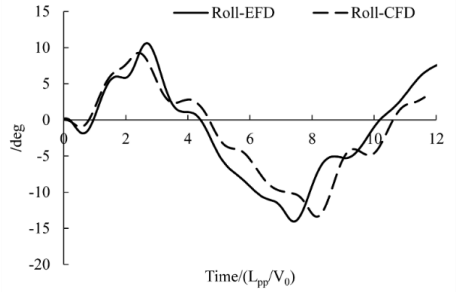

Figure 8 Roll motion for 10/10 zigzag maneuver

Figure 8 presents the comparison between the experimental and predicted roll for 10/10 zigzag maneuver. As we can see, the good agreement is obtained and both peak values are observed. The discrepancy of both peak values are -12.67% and 4.73%. The time of second peak value occurs later, compared with the experimental results. The roll and yaw rate are shown in Figure 9. They are related to the time to execute rudder. After starting to execute rudder, the yaw rate will quickly approach its maximum and then begin to decrease, while the roll rate varies slowly.

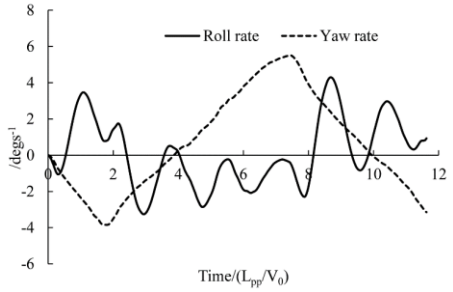

Figure 9 Time history of roll and yaw rate for 10/10 zigzag maneuver

Figure 10 shows the time history of rudder angle and yaw motion for 20/20 zigzag maneuver. And the predicted results of main parameters are listed in Table 4. The first overshoot angle is underestimated about 18.98%, while the error of the time to check yaw angle is overestimated about 1.57%. Compared with the experimental time to execute rudder, the predicted results lag gradually. The third time to execute rudder is over predicted about 3.94%. Figure 11 shows the experimental and predicted roll motion, which are in good agreement. The roll and yaw rates are presented in Figure 12. The yaw rate varies slowly after the second time to execute rudder.

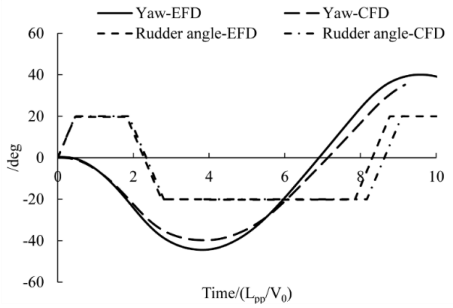

Figure 10 Time variation of rudder angle and yaw motion for 20/20 zigzag maneuver

Table 4 Comparison of main parameters for 20/20 zigzag maneuver

Parameters	EFD	CFD
1st OSA (deg)	24.40	19.77
T (1st OSA) (L_{pp}/V_0)	3.82	3.88
1st time to execute rudder (L_{pp}/V_0)	0	0
2nd time to execute rudder (L_{pp}/V_0)	2.78	2.80
3rd time to execute rudder (L_{pp}/V_0)	7.86	8.17

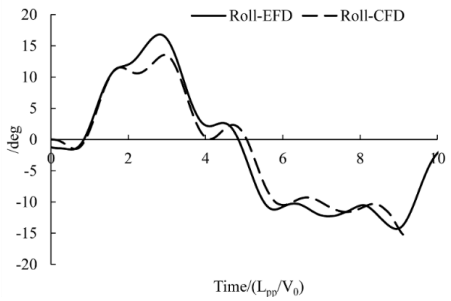

Figure 11 Roll motion for 20/20 zigzag maneuver

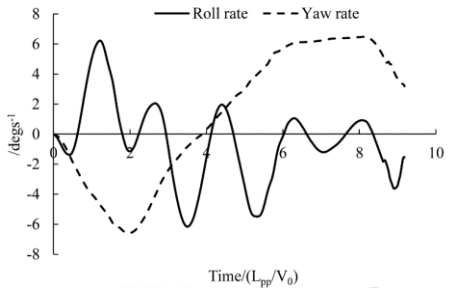

Figure 12 Time history of roll and yaw rate for 20/20 zigzag maneuver

The dimensionless magnitude of velocity, dynamic pressure and magnitude of vorticity are shown in Figure 14. When starting to execute rudder, the area of the high velocity zone is small on the starboard. And when ending to execute rudder, the area increases quickly and the range of high velocity near the hull translates to the starboard from the portside, and the velocity distribution is very complex. There is a small high velocity area near the root of the rudder, which is related to the vorticity. When the yaw motion approaches the maximum, the slipstream is more obviously in which the acceleration effection of the propeller ditermines the velocity distribution. When the rudder turns to the portside from the starboard, the low pressure zone on the starboard increases as shown in the middle in

Figure 14. When the rudder angle reaches to the second overshoot angle, the low pressure on starboard decreases, corresponding to the high velocity. The complex vorticity is presented at last. The variation of vorticity is similar to the dimensionless magnitude of velocity. A vertical high vorticity appears behind the rudder. During the rudder turns to portside, the high vorticity on the starboard increases gradually and the high vorticity near the root of the rudder translates to the starboard from the portside. At the maximum yaw angle, a high vorticity area occurs on the starboard.

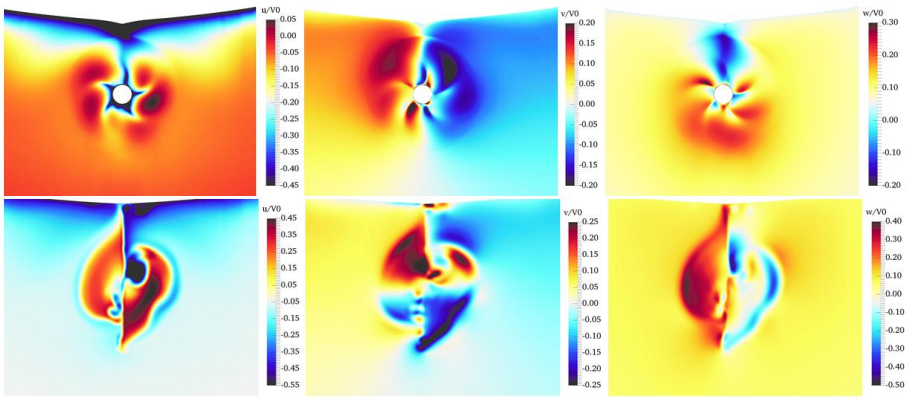
Figure 13 Wake field at x=0.9774L_{pp} (top) and 1.02L_{pp} (bottom) for self-propulsion (left: axial velocity; middle: lateral velocity; right: vertical velocity)

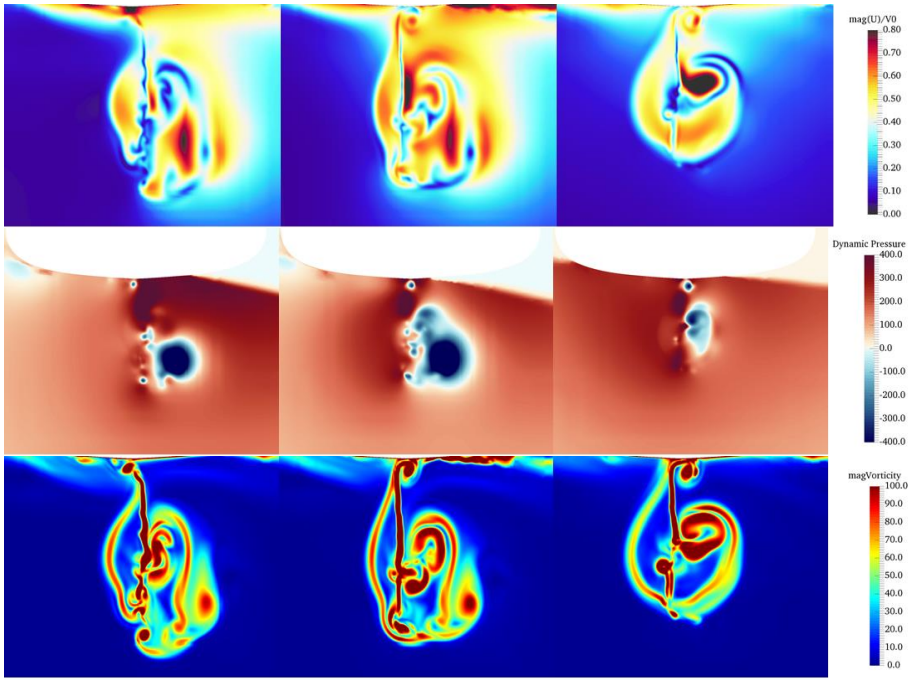

Figure 14 Dimensionless magnitude of velocity (top), dynamic pressure (middle) and magnitude of vorticity (bottom) Time history of roll and yaw rate for 10/10 zigzag maneuver at x=1.02L_{pp} (from left to right: A, B, C, as shown in Figure 7)

5. CONCLUSIONS

In the present study, the numerical simulations of self-propulsion and zigzag maneuver of KRISO Container Ship are carried out by naoe-FOAM-SJTU solver. The calculated conditions are setup according to the Benchmark test in SIMMAN 2020. The complex viscous flow field is simulated by coupling unsteady Reynolds averaged Niver-Stokes equations with the overset grid method, which is applied since the ship model is free to move in all directions.

In the calculation of self-propulsion, the rotating speed of the propeller is adjusted by PI controller. The heave and pitch motion are taken into consideration in the self-propulsion. The mean value of thrust in one period is about 58.72N and the rotating speed of propeller is about 12.44rps. In front of the propeller disk, the nonuniform wake field is accelerated obviously by the suction effect of the propeller. And the wake field of the propeller become more complex by the influence of the rudder. In the prediction of the zigzag maneuvering motion, the rotating speed of propeller is fixed according to the results of self-propulsion. There is a good agreement between the predicted results and experimental data regarding to the characteristic parameters such as overshoot angle, roll motion and the time to execute rudder. In both zigzag maneuver cases, the prediected results of second time to execute rudder lags behinds the experiment. This is because that the rudder attached to the hull is modified to facilitate the arrangement of overset grid. For the zigzag 10/10 cases, during the process of the second steering, the high speed region is mainly concentrated on the starboard; the corresponding is the low pressure region. And when the yaw angle approach to the maximum, the vorticity increases on the starboard.

In the future, DES model will be adopted to solve the flow field. And the results are going to be compared with that obtained by URANS model. The mechanism of hull-propeller-rudder interaction will be analyzed further and more detailed flow information will be investigated.

ACKNOWLEDGEMENTS

This work is supported by the National Natural Science Foundation of China (51879159), The National Key Research and Development Program of China (2019YFB1704200, 2019YFC0312400), Chang Jiang Scholars Program (T2014099), Shanghai Excellent Academic Leaders Program (17XD1402300), and Innovative Special Project of Numerical Tank of Ministry of Industry and Information Technology of China (2016-23/09), to which the authors are most grateful.

REFERENCES

[1] Stern, F., Kim, H.T., Patel, V.C., et al. A viscous-flow approach to the computation of propeller-hull interaction[J]. Journal of Ship Research, 32(4), pp. 246-262, 1988.

[2] Phillips, A.B., Turnock, S.R., Furlong, M. Evaluation of manoeuvring coefficients of a self-propelled ship using a blade element momentum propeller model coupled to a Reynolds averaged Navier Stokes flow solver[J]. Ocean Engineering, 36(15-16), pp.

1217-1225, 2009.
[3] Choi, J.-E., Kim, J.-H., Lee, H.-G., et al. Computational predictions of ship-speed performance[J]. Journal of Marine Science and Technology, 14(3), pp. 322-333, 2009.
[4] Choi, J.-E., Min, K.-S., Kim, J.H., et al. Resistance and propulsion characteristics of various commercial ships based on CFD results[J]. Ocean Engineering, 37(7), pp. 549-566, 2010.
[5] Lübke, L.O. Numerical simulation of the flow around the propelled KCS[C]. In the Proceedings of the CFD Workshop Tokyo 2005. Japan, pp. 587-592, 2005.
[6] Shen H L, Su Y M. Use of the sliding mesh technique to analyze interaction between ship hulls and propellers [J]. Journal of Harbin Engineering University. 31(1), pp. 1-7, 2010.
[7] Wang X, Cai F, Shi A G, Ying R R. Numerical simulation of the viscous flow over the ship with twin-propellers and twin-rudders in rotating arm tests [J]. Journal of Ship Mechanics. 18(7), pp. 786-793, 2014.
[8] Carrica, P.M., Stern, F. DES simulations of KVLCC1 in turn and zigzag maneuvers with moving propeller and rudder[C]. In Proceedings of SIMMAN 2008 Workshop on Verification and Validation of Ship Manoeuvering Simulation Methods. Lyngby, Denmark, 2008.
[9] Mofidi, A., Carrica, P.M. Simulations of zigzag maneuvers for a container ship with direct moving rudder and propeller[J]. Computers & Fluids. 96, pp. 191-203, 2014.
[10] Broglia, R., Dubbioso, G., Durante, D., et al. Turning ability analysis of a fully appended twin screw vessel by CFD. Part I: Single rudder configuration[J]. Ocean Engineering. 105, pp. 275-286, 2015.
[11] Dubbioso, G., Durante, D., Di Mascio, A., et al. Turning ability analysis of a fully appended twin screw vessel by CFD. Part II: Single vs. twin rudder configuration[J]. Ocean Engineering. 117, pp. 259-271, 2016.
[12] Muscari, R., Dubbioso, G., Viviani, M., et al. Analysis of the asymmetric behavior of propeller–rudder system of twin screw ships by CFD[J]. Ocean Engineering. 143, pp. 269-281, 2017.
[13] Shen, Z., Wan, D., Carrica, P.M. Dynamic overset grids in OpenFOAM with application to KCS self-propulsion and maneuvering[J]. Ocean Engineering. 108, pp. 287-306, 2015.
[14] Shen, Z., Ye, H., Wan, D. C. URANS simulations of ship motion responses in long-crest irregular waves[J]. Journal of Hydrodynamics, Ser. B. 26(3), pp. 436-446, 2014.
[15] Shen, Z., Wan, D. C., Carrica, P.M. RANS simulations of free maneuvers with moving rudders and propellers using overset grids in OpenFOAM[C]. In Proceedings of SIMMAN 2014 workshop on Verification and Validation of Ship Maneuvering Simulation Methods. Lyngby, Denmark, 2014.
[16] Shen, Z., Wan, D. C. An irregular wave generating approach based on naoe-FOAM-SJTU solver[J]. China Ocean Engineering. 30, pp. 177-192, 2016.
[17] Wang, J., Zhao, W., Wan, D. C. Free Maneuvering Simulation of ONR Tumblehome Using Overset Grid Method in naoe-FOAM-SJTU Solver[C]. In Proceedings of 31th Symposium on Naval Hydrodynamics. Monterey, USA, 2016.
[18] Wang J H, Zou L, Wan D C, CFD simulations of free running ship under course keeping control, Ocean Engineering, 141, pp. 450-464, 2017.
[19] Wang J H, Zhao W W, Wan D C, Simulations of Self-Propelled Fully Appended Ship Model at Different Speeds, International Journal of Computational Methods. 16(5), pp. 1840015-1 -1840015-22, 2019.
[20] Berberović, E, van Hinsberg, NP, Jakirlić, S, et al. “Drop impact onto a liquid layer of finite thickness: dynamics of the cavity evolution,” *Phys Rev E*, 79(3), 36306, 2009.